Wetting and Prewetting on Ceramic Surfaces

Jian Luo[1] and Yet-Ming Chiang[2]

[1] School of Materials Science and Engineering, Center for Optical Materials Science and Engineering Technologies, Clemson University, Clemson, South Carolina 29634; email: jianluo@clemson.edu

[2] Department of Materials Science and Engineering, Massachusetts Institute of Technology, Cambridge, Massachusetts 02137; email: ychiang@mit.edu

Key Words

surficial amorphous films, intergranular films, equilibrium thickness, premelting, multilayer adsorption

Abstract

The stabilization of nanoscale surficial amorphous films (SAFs) for Bi_2O_3 on ZnO, VO_x on TiO_2, SiO_x on Si, and several other oxide systems provides evidence for the existence of prewetting phenomena with analogies in water and other simple systems, as well as the stabilization of intergranular amorphous films in ceramics. Experimental results show that in the subeutectic regime, the equilibrium film thickness decreases monotonically with decreasing temperature until it vanishes at a dewetting (prewetting) temperature. With increasing temperatures, nanometer-thick SAFs persist into a solid-liquid coexistence regime, in equilibrium with partial-wetting drops, with a gradual decrease in the macroscopic contact angle upon heating. The presence of an attractive dispersion force can significantly delay or inhibit the (otherwise expected) occurrence of complete wetting at higher temperatures. The equilibrium thickness of SAFs is explained from a balance between several interfacial interactions, including dispersion forces, short-range forces of structural or chemical origins, volumetric free-energy terms, and electrostatic interactions. In a generalized Cahn critical-point wetting model, these SAFs are alternatively considered to be disordered multilayer adsorbates formed from coupled prewetting and premelting transitions.

INTRODUCTION

IGF: intergranular (glassy) film

GB: grain boundary

HRTEM: high-resolution transmission electron microscopy

SAF: surficial amorphous film

Impurity-based, equilibrium-thickness intergranular films (IGFs) have been widely observed at ceramic grain boundaries (GBs) (1–5), ceramic-ceramic heterointerfaces (4, 5), metal-oxide heterointerfaces (6–11), and metallic GBs (5, 12, 13), through the use of high-resolution transmission electron microscopy (HRTEM). Recently, free-surface counterparts to these IGFs have been found for Bi_2O_3 on ZnO $\{11\bar{2}0\}$ surfaces (14–17), VO_x on TiO_2 anatase (101) surfaces (18), SiO_x on Si (19), and several other oxides (10, 15, 16). We refer to these as surficial amorphous films (SAFs), although partial order generally exists within the films.

Like IGFs, these SAFs are understood to be quasi-liquid layers that adopt an equilibrium thickness on the order of 1 nm (5, 14–17). From the viewpoint of wetting, SAFs are considered to be an intermediate regime between Langmuir submonolayer adsorption and complete wetting (2, 3, 5, 16, 17). We (5, 16, 17, 20) have proposed that these SAFs can alternatively be considered as disordered multilayer adsorbates that form from coupled prewetting (21) and premelting (22–24) transitions under the framework of a generalized Cahn critical-point wetting model (21). Unique anisotropic wetting behavior with and without nanometer-thick SAFs has been observed (25). This article reviews the experimental observations of, and models for, SAFs and related wetting phenomena on ceramic surfaces.

BACKGROUND

Wetting

If partial wetting (or nonwetting) takes place, the contact angle is given by Young's equation:

$$\gamma_{cv} = \gamma_{lv} \cdot \cos\theta + \gamma_{cl}, \qquad 1.$$

where γ_{cl}, γ_{lv}, and γ_{cv} are the excess free energies for crystal-liquid, liquid-vapor, and crystal-vapor interfaces, respectively. Some adsorption of the liquid species on the surface is generally expected. If the surface excess (Γ) is positive, γ_{cv} is reduced according to the Gibbs isothermal equation ($d\gamma = -\Gamma \cdot d\mu$). Thus, γ_{cv} is generally smaller than $\gamma_{cv}^{(0)}$, the excess free energy of a "clean" surface with $\Gamma = 0$.

If complete (or perfect) wetting takes place, the excess surface free energy is given by (26)

$$\gamma_{cv} \equiv \gamma_{lv} + \gamma_{cl}. \qquad 2.$$

Furthermore, first-order or critical (continuous) wetting transitions can occur (26). de Gennes (27), Dietrich (28), and Bonn and Ross (26) have comprehensively reviewed wetting phenomena and theories.

Prewetting

Prewetting, which refers to a wetting transition occurring when the phase that does the wetting is not yet stable (26), leads to the formation of thicker adsorption layers (which are still of microscopic thickness). Prewetting transitions were initially proposed in the Cahn critical-point wetting model (21) for demixed liquids, and such transitions have been confirmed in organic systems (29, 30) and in the Pb-Ga liquid metal system (31, 32). As the temperature rises and approaches the bulk critical point, a first-order complete wetting transition is predicted in the two-phase region within the miscibility gap (**Figure 1**). Furthermore, this model predicts a prewetting line in the single-phase region (**Figure 1a**), representing first-order transitions from low- to high-adsorption interfacial structures (**Figure 1c**). The prewetting line terminates at a surface critical point where
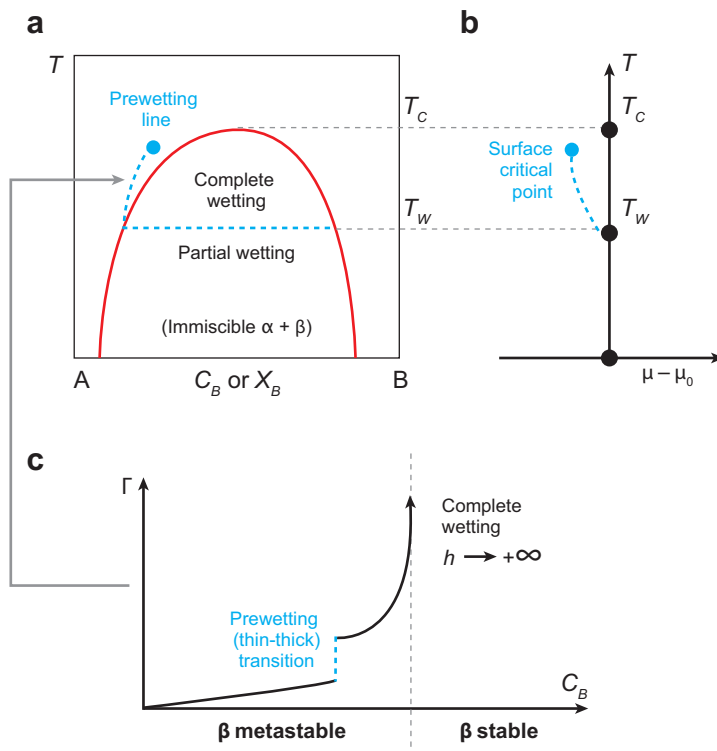
Figure 1

(*a*) Schematic illustration of the Cahn critical-point wetting model for binary demixed liquids, in which a complete wetting tie line in the two-phase region extends into the single-phase region as a first-order prewetting line. (*b*) An alternative representation of the critical-point wetting diagram. (*c*) Surface solute excess versus the overall composition at the temperature indicated by the arrow in panel *a*.

the difference between low- and high-adsorption interfacial structures vanishes. The prewetting model and critical-point wetting model are adapted to represent vapor adsorption on chemically inert substrates near the liquid-vapor critical point through the use of a diffuse-interface theory that is isomorphic to Cahn's original theory (5, 26, 33). Wetting transitions for ionic liquids have also been studied (34).

Premelting

Premelting, or surface melting, refers to the stabilization of a surface quasi-liquid layer below the bulk melting temperature. This phenomenon has been confirmed experimentally for ice, Pb, and other unary systems. The theories and experiments of premelting have been reviewed (22–24, 35). When complete premelting occurs, the thickness of the surface quasi-liquid layer increases continuously with increasing temperature until the layer thickness diverges at the bulk melting temperature. In contrast, when incomplete premelting occurs, a surface premelting layer of microscopic thickness forms at the solid-liquid-vapor triple point in equilibrium with a partial-wetting liquid drop (23, 24).

Interfacial premelting at ice-Si (36) and Pd-Al (37) heterointerfaces has also been observed. GB premelting was suggested by atomistic simulations of metals (38, 39) and Si (40, 41), a continuum

model of ice (42), and generic diffuse-interface models (43, 44). However, in situ hot-stage transmission electron microscopy (TEM) experiments in Al concluded that GB premelting likely occurs only at $>0.999\ T_{\text{melting}}$ (45). Recently, GB premelting in colloidal crystals was revealed (46).

Although premelting is rigorously defined only for unary systems, Tang et al. (20) recently suggested the existence of GB adsorption transitions that are coupled with localized structural disorder transitions, i.e., coupled GB premelting and prewetting transitions, in binary alloys. An analogous theory was proposed for SAFs (17).

TEM: transmission electron microscopy

Impurity-Based Equilibrium-Thickness Intergranular Films

A unique class of nanometer-thick IGFs has been widely observed at GBs and heterophase interfaces in ceramics (for a review, see Reference 5). Clarke and colleagues (1, 47) initially proposed that these IGFs adopt an equilibrium thickness in response to a balance between several attractive and repulsive interfacial interactions. Interfacial forces at play include London dispersion forces (which are always attractive for IGFs) (48), short-range repulsions of structural and chemical origins (1, 49, 50), electrostatic interactions (47), volumetric free-energy terms (5, 15–18, 51), and capillary and applied pressures (1, 47).

Silicate-based IGFs of similar character have also been observed at metal-oxide interfaces (6–11, 52). Although nanoscale disordered GB structures in metals (i.e., metallic IGFs) are not widely found by HRTEM, GB structural transitions were indicated by measured discontinuities or abnormalities in macroscopic properties (5). Among all systems, Cu-Bi (53–58) and Fe-Si-Zn (55, 59–62) have been most systematically studied. Recently, direct HRTEM evidence for the existence of nanoscale metallic IGFs has been obtained for Ni-doped W, and these quasi-liquid films form at subeutectic temperatures (12, 13).

Cannon and colleagues (2, 3) critically assessed IGFs in several ceramic systems. In a recent review, Luo (5) evaluated the equilibrium-thickness IGFs in ceramics; their metallic and free-surface counterparts (the latter are SAFs); and their relations to simpler phenomena of prewetting, premelting, and frustrated-complete wetting. That review also attempts to establish a unifying thermodynamic framework. In the following, we consider several systems in which evidence for the stabilization of SAFs is quite clear.

EXPERIMENTAL OBSERVATIONS

Bi_2O_3-Enriched Surficial Amorphous Films on ZnO $\{11\bar{2}0\}$ Surfaces

Bi_2O_3-enriched SAFs formed on ZnO $\{11\bar{2}0\}$ surfaces have been extensively characterized. We briefly summarize the following experimental observations, which were reported in References 14–16.

SAFs found on the $\{11\bar{2}0\}$ surfaces of Bi_2O_3-doped ZnO particles have nearly constant thickness at a fixed temperature and chemical potential (15). As in the case of IGFs, the film thickness is nearly constant along the surface (**Figure 2a**). For example, measurement of 97 films in Bi_2O_3-saturated ZnO annealed at 780°C yielded a mean value for the film thickness of 1.54 nm with a standard deviation of 0.28 nm (15). Once an equilibrium state has been reached, variations in additional annealing time and the amount of bulk second phase have no discernible influence on the average value of, or variability in, film thickness (**Figure 2b**) (15). Thus, these SAFs have an equilibrium thickness at constant temperature and bismuth oxide activity.

Auger electron spectroscopy showed that the nanoscale SAFs are markedly enriched in ZnO compared with the equilibrium bulk liquid. The average measured composition of the film formed
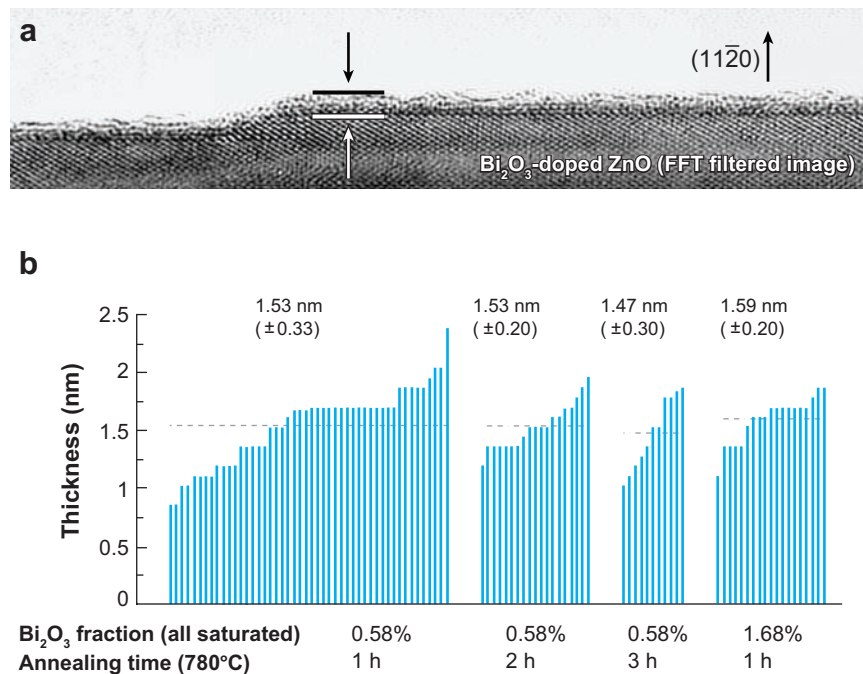
Figure 2

(*a*) HRTEM image of an SAF with constant thickness. The film is ~1.5 nm thick. (*b*) Film thickness versus equilibration time and Bi_2O_3 excess for Bi_2O_3 on ZnO at 780°C. Each bar represents one measured thickness. Doping levels of 0.58 mol.% and 1.68 mol.% both represent saturated samples in which the chemical potentials are the same. Reprinted from Reference 15 with permission from Elsevier.

at 780°C is 18 mol.% Bi_2O_3 (i.e., ~44 vol.% Bi_2O_3 or a Bi/Zn ratio of 0.43), whereas the near-eutectic equilibrium bulk liquid contains ~83 mol.% Bi_2O_3 (i.e., 94 vol.% Bi_2O_3 or a Bi/Zn ratio of 9.8) at the same temperature (15). A schematic illustration of the equilibrium surface wetting and adsorption configuration for a Bi_2O_3 liquid drop on a ZnO $\{11\bar{2}0\}$ surface at 780°C is shown in **Figure 3*a***.

Furthermore, SAFs with similar character can be observed in Bi_2O_3-saturated samples equilibrated above the bulk eutectic temperature (740°C), where they are in equilibrium with ZnO substrates and nonwetting bulk liquid drops, and below the bulk eutectic temperature, where they are in equilibrium with two crystalline bulk phases in a binary system, as well as in single-phase samples containing concentrations of Bi_2O_3 below the bulk solid solubility limit (**Figure 4*a***) (15, 16).

To identify any kinetic limitations to equilibration, the SAFs in a saturated sample were allowed to approach their equilibrium state from both lower and higher temperatures. **Figure 4*b*** shows reversible temperature dependence to the film thickness for saturated samples. The film thickness decreases monotonically with decreasing temperature in the subeutectic range. To seek the complete dewetting of SAFs, a saturated sample was first fired at 780°C, at which equilibrium SAFs are known to form, and then annealed at 450°C for six months (4392 h). This prolonged annealing experiment showed that the SAF does dewet the surface at 450°C (16). Moreover, the SAFs are thinner in unsaturated specimens within the bulk single-phase region (**Figure 4*b***).

Although none of the films appear to be fully crystalline, most quenched films exhibit some degree of layering and lateral order (16). A layered structure was frequently observed (**Figure 5*a***).
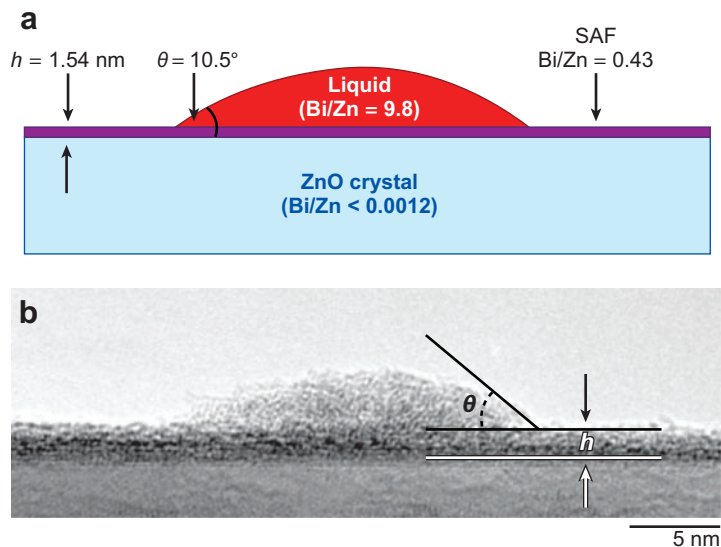
Figure 3

(*a*) Schematic illustration of the equilibrium surface wetting and adsorption configuration for a Bi_2O_3-rich drop on a ZnO {11$\bar{2}$0} surface at 780°C (15, 25). (*b*) HRTEM image of a nanometer-thick SAF coexisting with a partial-wetting nanodroplet in the Bi_2O_3 on ZnO system at 700°C. Panel *b* is reprinted from Reference 16 with permission from American Chemical Society.

Occasionally, lateral ordering (**Figure 5b**) with a period doubling the ZnO {1$\bar{1}$00} lattice space was also observed. The period of this lateral partial order (**Figure 5b**) is roughly equal to the lattice constant of cubic δ-Bi_2O_3 (0.565 nm) (15). However, structure and composition analysis reveals that these films are not simply epitaxial layers of the δ-Bi_2O_3 phase expected in bulk coexistence (15). If one assumes that the order does not entirely occur during the quench, this observation supports the induced-order hypothesis in the original Clarke model (1) and recent diffuse-interface theories (20, 44). The two images shown in **Figure 5** represent the most ordered, rather than the typical, observed films.

In summary, nanometer-thick SAFs formed on Bi_2O_3-doped ZnO {11$\bar{2}$0} facets exhibit

1. similar character in three different regimes of bulk phase coexistence,
2. an equilibrium thickness that depends on equilibration temperature and Bi_2O_3 chemical potential,
3. high structural disorder, even at subeutectic and undersaturation conditions, and
4. a distinct composition highly enriched in ZnO compared with the equilibrium bulk liquid.

A second class of thicker films coexisting with nanodroplets (5–15 nm) of Bi_2O_3-rich liquid or glass (**Figure 3b**) has also been observed in the same materials, but only on a small fraction of the particle surfaces (16). This behavior was interpreted as a case of metastable (local) equilibration in a closed system in which the total surface excess is restricted by the relatively slow evaporation kinetics for moving excess Bi_2O_3 to the secondary phase regions, but the amorphous phase can still redistribute locally through surface diffusion to lower the free energy. Further analysis (16) suggests that the larger, temperature-insensitive thickness exhibited by this second class of SAFs represents a case in which the attractive interaction resulting from a volumetric free-energy term is diminished. **Figure 3b** directly illustrates that the liquid does not wet the quasi-liquid surface layer.
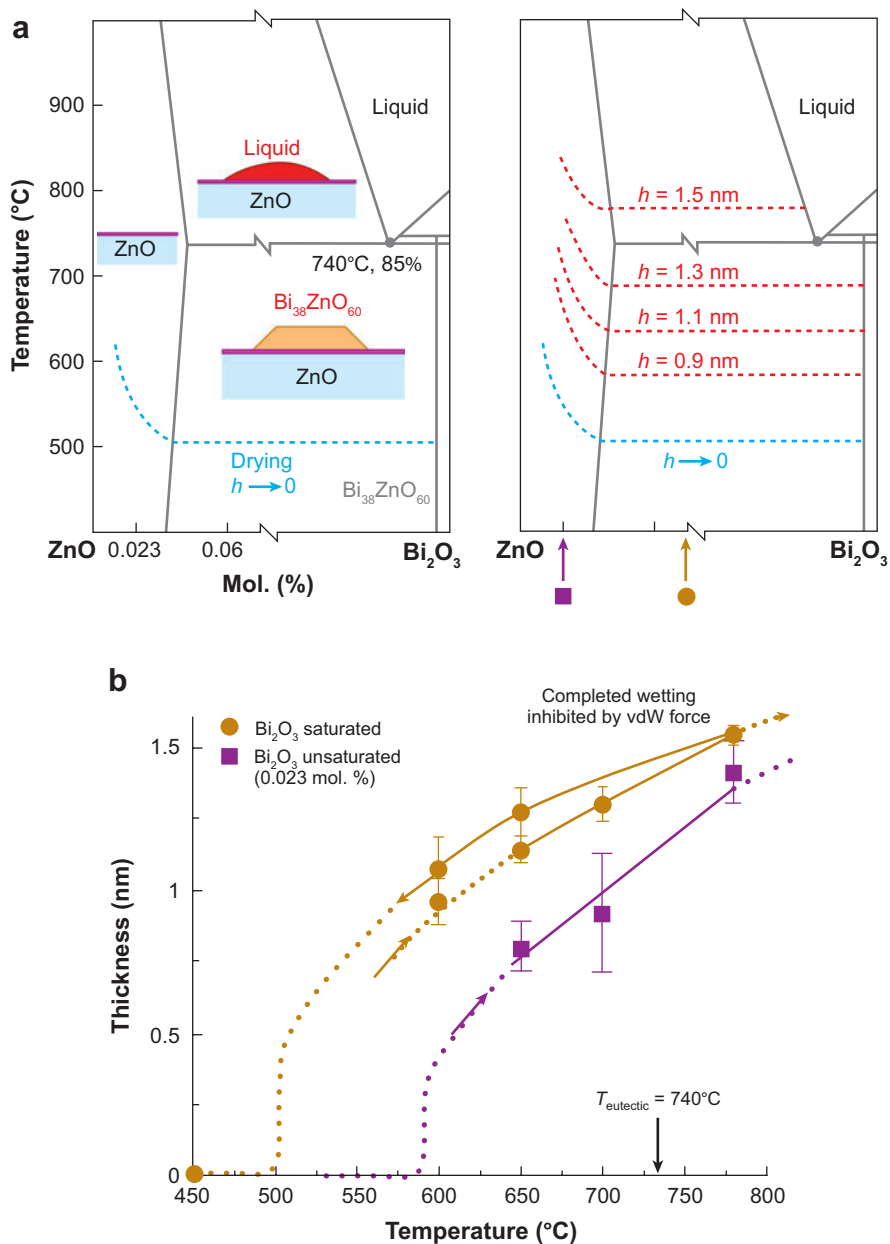
Figure 4

(*a*) Schematic illustrations of observed Bi_2O_3-enriched SAFs on ZnO {11$\bar{2}$0} surfaces in the phase regions of the ZnO-Bi_2O_3 binary bulk phase diagram. In the diagram on the right, lines of constant film thickness (*red dashed lines*) are plotted in the same bulk phase diagram. (*b*) Average thicknesses versus temperature in Bi_2O_3-saturated (*yellow lines*) and Bi_2O_3-unsaturated (*purple line*) samples. For saturated samples, the equilibration was approached from both higher and lower temperatures, demonstrating reversible temperature dependence of film thickness. This figure was replotted by combining data from References 15–17 and 25.
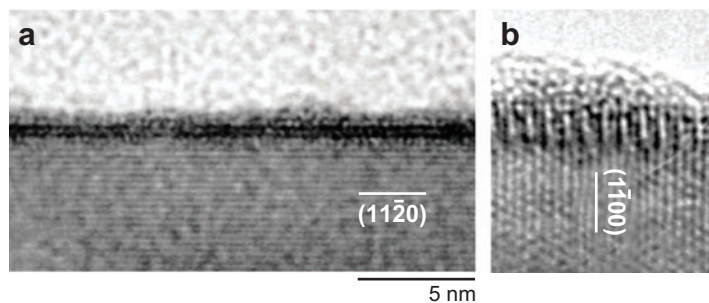
Figure 5

Partial order was observed in quenched films, including (*a*) layering structure and (*b*) lateral order whose period doubles the ZnO {1$\bar{1}$00} lattice distance. In panel *b*, the sample is aligned to show the parallel ZnO {1$\bar{1}$00} lattice fringes and is slightly tilted around the perpendicular ⟨11$\bar{2}$0⟩ axis to show the lateral ordering clearly. Reprinted from Reference 16 with permission from American Chemical Society.

VO$_x$-Based Surficial Amorphous Films on TiO$_2$ Anatase (101) Surfaces

Thermal spreading of V$_2$O$_5$, MoO$_3$, and other catalytic oxides onto the surfaces of refractory oxide supports (e.g., Al$_2$O$_3$ or TiO$_2$) is widely used to disperse metal oxide catalysts (63–68). It was previously thought that monolayer surface adsorption occurs during the spreading process (64, 65). However, a recent study (25) found equilibrium-thickness SAFs, akin to those observed for Bi$_2$O$_3$ on ZnO, in a model catalyst system: VO$_x$ on TiO$_2$ (63–68). In this system, SAFs with similar character formed on several faceted surface orientations as well as on curved surfaces of both anatase and rutile particles.

A systematic investigation of SAFs formed on anatase (101) surfaces was pursued. A typical HRTEM image of a VO$_x$-based SAF formed on the anatase (101) surface is shown in **Figure 6a**. These SAFs also exhibit a self-selecting or equilibrium thickness. The average thickness for 119 SAFs that formed at 600°C is 1.10 nm, with a standard deviation of 0.26 nm. Furthermore, the results in **Figure 6b** show that the film thickness is virtually independent of nominal V$_2$O$_5$ loading (the amount of excess bulk V$_2$O$_5$ secondary phase), annealing time (after an initial transient), and the synthesis method, indicating a thermodynamically determined thickness analogous to the results in **Figure 2b** for Bi$_2$O$_3$-enriched SAFs on ZnO {11$\bar{2}$0} facets.

The temperature dependence of film thickness (**Figure 6c**) shows interesting behavior. Upon heating, there is a discontinuous transition from submonolayer to multilayer coverage between 500°C and 550°C. Upon cooling, the transition back to submonolayer coverage occurs at ∼50°C lower. Outside the temperature range of this hysteresis, the coverage/film thickness is reversible. The hysteresis and discontinuous change in thickness suggest a first-order monolayer-to-multilayer surface adsorption transition.

Although these SAFs formed at subeutectic/subsolidus conditions (69), they, like the Bi$_2$O$_3$-enriched films on ZnO, are at least partially disordered when observed by HRTEM (**Figure 6a**). However, digital image analysis of one HRTEM image has shown partial ordering in an SAF with a periodicity that matches the interlayer distance in the V$_2$O$_5$ crystal structure (25). Here also, it is not certain whether order increases during the quench. A premelting-like force-balance model (in which the fusion entropy of pure V$_2$O$_5$ is used to estimate the amorphization energy) results in thickness-versus-temperature values that agree reasonably well with experiment (**Figure 6c**), although there is no provision in the model for the submonolayer-to-multilayer transition.
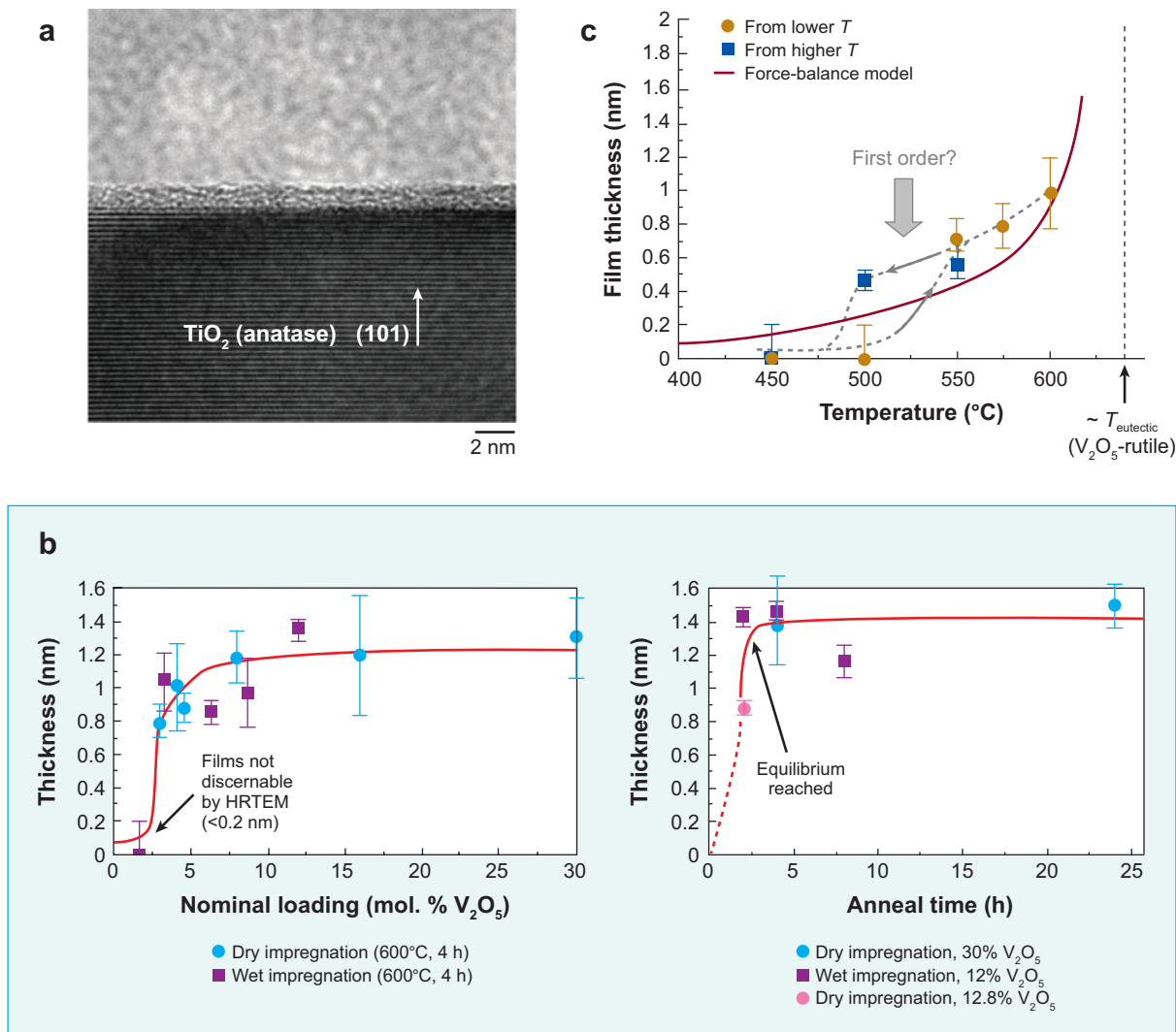
234   *Luo • Chiang*

Figure 6

(*a*) HRTEM image of a vanadia-based SAF formed at 600°C. (*b*) The measured film thickness is independent of the additional anneal time, the V_2O_5 loading, and synthesis methods after thermodynamic equilibrium states are reached. (*c*) Average film thickness versus equilibration temperature for two sets of specimens: one in which the equilibrium state was approached from lower temperatures and one in which the equilibrium state was approached from higher temperatures. A force-balance model was used to compute the solid line. Reprinted from Reference 18 with permission from American Institute of Physics.

Surficial Amorphous Films in Other Systems

Limited data support the existence of nanoscale SAFs in several other systems. MoO_3 on Al_2O_3 is another supported oxide catalyst system that exhibits SAFs with a similar trend in temperature-dependent stability as those discussed in the two systems above (16). At low firing temperatures of 450–650°C, no distinguishable films were observed by HRTEM (**Figure 7***a*), although surface segregation of Mo was confirmed by energy-dispersive X-ray spectroscopy (EDXS) (16). After firing at higher temperatures (900–975°C, $T_{melting} = 795°C$ for MoO_3), a bilayer adsorbate of
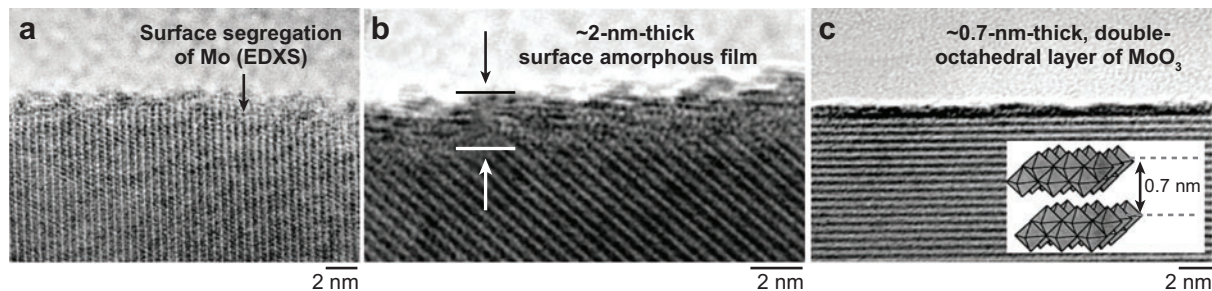
EDXS: energy-dispersive X-ray spectroscopy

Figure 7

(*a*) A "dry" surface with Mo segregation within or on the Al_2O_3 crystal structure observed in a lower temperature range (450–650°C). At higher temperatures (900–1000°C), (*b*) 1–2-nm-thick surface amorphous films are formed on a small fraction of surfaces, and (*c*) double-octahedral, adsorbed layers of MoO_3 or one layer of the α-MoO_3 structure, as shown in the inset, are formed on a large fraction of surfaces. Adapted from Reference 16 with permission from American Chemical Society.
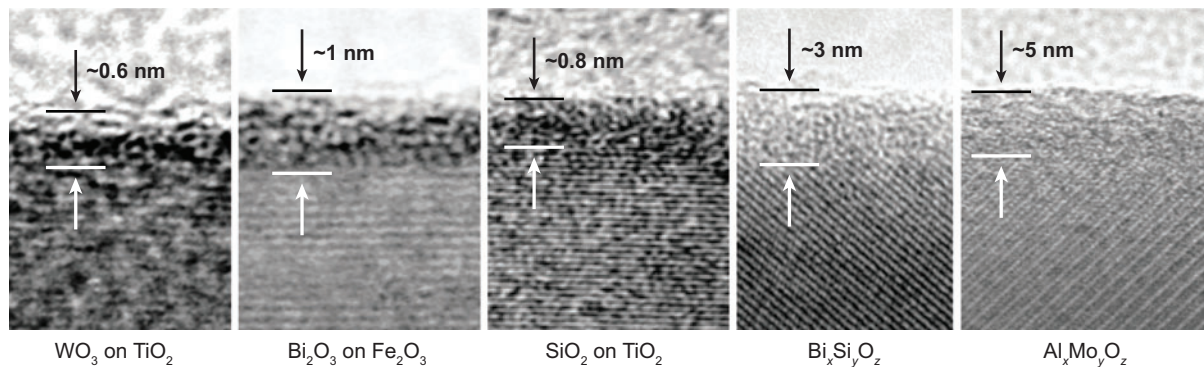

Figure 8

HRTEM images for the widespread existence of SAFs in two-component oxides.

~0.7 nm thickness, which coincides with the double-octahedral-layer thickness of the α-MoO_3 structure, was observed on a large portion of surfaces (**Figure 7*c***). In a few instances (<5% of all Al_2O_3 surfaces), 1–2-nm-thick SAFs were also observed (**Figure 7*b***); for a subset of these, a nanosized partial-wetting droplet of Mo-rich amorphous material was also present nearby (16). Thus, this one system appears to exhibit three distinct adsorption configurations. Nanometer-thick, silicate-based SAFs have also been observed on Al_2O_3 substrates, in equilibration with partially wetted anorthite (10).

Incidental observations of SAFs in several other oxides are shown in **Figure 8**; in each instance the crystalline bulk phase is labeled. For at least two of these instances, the London dispersion interaction across the film corresponds to an estimated negative Hamaker constant (A_{123}) and should act to thicken the SAF (15). These examples include the ~0.9-nm-thick, Bi_2O_3-enriched SAFs on Fe_2O_3 at 800°C ($T_{eutectic}$ = 960°C; A_{123} = −29 zJ) and the ~0.66-nm-thick WO_3-enriched SAFs on TiO_2 at 1100°C ($T_{eutectic}$ = 1233°C; A_{123} = −105 zJ). For these as well as other cases in which SAFs are observed at subeutectic temperatures, we now presume that the volume free-energy penalty for forming (binary) undercooled liquids is significant in providing the attractive interaction that prevents unlimited thickening of the films, analogous to the case of

premelting in unary systems, although attractive or repulsive London dispersion interactions as
originally proposed for IGFs (1, 47) may of course also contribute. Conversely, the volume energy
contribution should also be taken into account in interpreting IGF behavior, depending on the
system in question.

Another system in which equilibrium-thickness SAFs have recently been stabilized via ther-
modynamic control is the surface oxide on Si (19; E. Jud, M. Tang & Y.-M. Chiang, unpublished
work). Here, oxygen is treated as the impurity, and by the use of ultralow oxygen partial pressures
generated through equilibration with metal/metal oxide buffer systems, the formation of SiO_x
and Hf-Si-O films (of interest to the gate-oxide field) at partial pressures in the vicinity of the
bulk SiO_2/Si coexistence value (e.g., $\sim 10^{-40}$ atm at 700°C) can be studied. Regimes of constant
film thickness over many decades of oxygen partial pressure, including above the bulk coexis-
tence value, are reported. Divergence to fully wetting films is presumed to occur at still higher
oxygen activity, although observation of wetting in the presence of active oxidation processes is
difficult.

Although not generally interpreted in the same manner as the films we discuss here, other in-
stances of nanometer-thick amorphous films have been reported at the surfaces of various nanopar-
ticles and nanowires (70–74). Most of these films are likely to have formed under nonequilibrium
conditions.

Anisotropic Wetting of Surficial Amorphous Films: Bi$_2$O$_3$ on ZnO

The anisotropic formation of Bi_2O_3-enriched SAFs on ZnO (**Figure 9a**) provides a unique ex-
perimental opportunity to examine wetting behavior with and without the presence of nanoscale
SAFs (25). Such experiments are useful for probing the temperature dependence of SAF stability
and provide key information for the thermodynamic models discussed in the following section.
Figure 9a shows this anisotropy in SAF formation: Although no film has been observed to form
on ZnO surfaces of {$1\bar{1}00$} orientation, facets with associated films are almost always observed at
the {$11\bar{2}0$} surface. The anisotropy has been attributed to induced order between this ZnO surface
and bismuth oxide structural units constituting the film (**Figure 9b**) (15).

The contact angles of Bi_2O_3-rich liquid droplets and their temperature dependences differ
strikingly between these two surface orientations. The simpler behavior occurs at the ZnO {$1\bar{1}00$}
surface, where the measured contact angle of Bi_2O_3-rich droplets is virtually constant over a wide
temperature range from 700°C to 1000°C and has a value of 14.6° (**Figure 9c**). The behavior at the
ZnO {$11\bar{2}0$} surface, where the droplet is in contact with a nanometer-thick SAF (**Figure 9a**) (15),
is more complex but also shows an absence of complete wetting up to quite high temperatures.
The contact angle is smaller overall and decreases monotonically with increasing temperatures
between $\sim$750°C and $\sim$860°C before leveling off at a constant value above $\sim$860°C (25). The
mean contact angle in the high temperature regime between 900°C and 1000°C is 6.0° (**Figure 9c**).
Receding drop kinetics on this surface show a unique two-stage behavior, the analysis of which also
shows that complete wetting does not occur up to temperatures as high as 1050°C. The receding
contact angle was estimated to be $\sim$4° via two methods (25). Thus, the true Young's contact angle
for a Bi_2O_3-rich liquid drop on the ZnO {$11\bar{2}0$} surface (in equilibrium with a nanoscale SAF) is
between 4° and 6° over the temperature range 900–1050°C (25). These results are further analyzed
below. Additional details regarding the effects of heating rate, drop composition, hysteresis, and
faceted ridges forming at the triple lines are discussed in Reference 25.

Related results have been obtained for Ge-Pb liquid drops on the Pb solid surface, in which
wettability was enhanced on the facets that premelt, and the enhancement is absent at temperatures
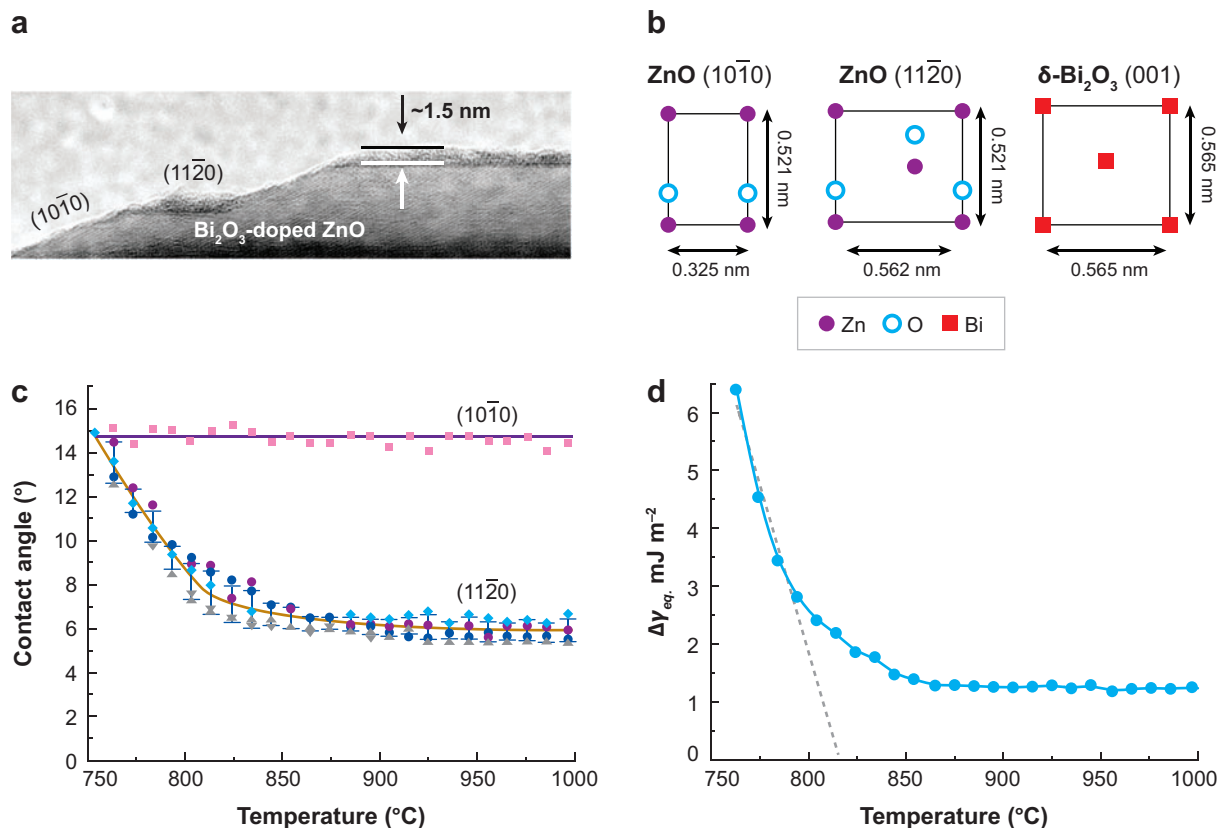lower than that at which Pb premelting occurs (75, 76).

Figure 9

(*a*) HRTEM image of anisotropic formation of nanometer-thick SAFs in Bi_2O_3-doped ZnO (14, 15). (*b*) Schematic illustration of the first plane of atoms terminating the $\{11\bar{2}0\}$ and $\{1\bar{1}00\}$ ZnO surfaces along with the plane of δ-Bi_2O_3. (*c*) Contact angle versus temperature measured for Bi_2O_3 on ZnO $\{11\bar{2}0\}$ and $\{1\bar{1}00\}$ surfaces (25). (*d*) Calculated $\Delta\gamma_{eq.}$ versus temperature for Bi_2O_3 on ZnO $\{11\bar{2}0\}$ surfaces. Linear extrapolation from the data between 750°C and 800°C would project a first-order complete wetting transition at 818°C. However, the occurrence of complete wetting is inhibited, and the observed residual $\Delta\gamma_{eq.}$ can be quantitatively explained from the magnitude of a long-range attractive London dispersion force (25).

THERMODYNAMIC MODELS

Analogous Phenomena

Thermodynamic models for SAFs in multicomponent inorganic materials can be developed from basic physical concepts underlying several well-known interfacial phenomena. The stabilization of SAFs under low-temperature conditions in which the bulk binary liquid phase is not stable has clear analogies to premelting and prewetting. If an additional attractive interfacial interaction (e.g., a long-range dispersion force) is present to limit the SAF thickness, SAFs can persist to higher temperatures in the solid-liquid coexistence regime, in equilibrium with a partially wetting liquid, invoking an analogy to the phenomenon of frustrated-complete wetting (77). The term prewetting generally has been used to refer to those cases in which the phase that does the wetting is metastable. However, there is uncertainty as to how to refer to cases in which the complete wetting transition either is delayed to well above the bulk eutectic temperature or is completely inhibited,

INTERFACE-STABILIZED QUASI-LIQUID FILMS

The SAFs discussed in this review are a subclass of interface-stabilized quasi-liquid films that have been observed in ceramics, metals, and molecular solids. Another well-known example of such films is impurity-based IGFs in ceramics, which are discussed in the Background section above. Recently, metallic counterparts to these IGFs in ceramics have been observed (12, 13), showing the ubiquitous existence of analogous interfacial phenomena. Furthermore, these quasi-liquid interfacial films are stabilized at subeutectic and undersaturated conditions, suggesting analogies to the well-known but simpler phenomena of premelting (22) and prewetting (21). These nanoscale quasi-liquid films can also persist into the solid-liquid coexisting regimes, in equilibration with partial-wetting bulk liquid drops (of markedly different composition), for which an analogy to the phenomenon of frustrated-complete (or pseudo-partial) wetting can be made. These nanoscale interfacial films can alternatively be understood to be equilibrium-thickness quasi-liquid layers in a high-temperature colloidal theory (1) or multilayer adsorbates with compositions and interfacial solute excesses set by bulk chemical potentials (3). In a recent review (5), equilibrium-thickness IGFs in ceramics, along with their free-surface counterparts (i.e., SAFs) and their metallic counterparts, are critically assessed under a unifying thermodynamic framework.

as the data for Bi_2O_3 on ZnO suggest may occur, or to those cases in which the character of the SAFs in the solid-liquid coexistence region is not distinctly different from those SAFs formed at subsolidus/subeutectic conditions. Under the expectation that there exists some condition (e.g., sufficiently high temperatures) in which complete wetting does occur, it is conceptually useful to consider the nanoscale SAFs as prewetting films (3), and we adopt that terminology in what follows. These SAF films (as well as the prewetting films in Cahn's original critical-point wetting model for binary liquids) are multilayer adsorbates that obey the Gibbs adsorption theory.

Like IGFs, SAFs alternatively can be modeled through the use of diffuse-interface and force-balance theories, which are discussed in detail in the following two sections. Diffuse-interface theories consider through-thickness compositional and structural gradients; an equilibrium configuration is obtained via minimization of an excess free-energy integral that include both volumetric and gradient thermodynamic terms. In simplified force-balance models, gradient energies, along with part of the coupled volumetric thermodynamic energies (5), are largely included in the short-range forces of structural and chemical origin. Such a simplified treatment (i.e., expressing excess film free energy as a function of film thickness and neglecting the through-thickness gradients except for the approximations used for deriving interfacial forces) will allow additional interfacial interactions, such as London dispersion and electrostatic (double-layer) forces, to be conveniently incorporated. In force-balance models, the disjoining pressure (which is defined as the derivative of excess film free energy with respect to the film thickness) is a sum of multiple attractive or repulsive interfacial forces/pressures (which are often anaalogous to those interparticle forces in collodial theories or IGF models), and the film adopts an equilibrium thickness (as well as an average composition) that minimizes the excess free energy. Equilibrium SAFs are (multilayer) adsorbates with surface solute excesses set by bulk chemical potentials, and both diffuse-interface and force-balance models are fully consistent with the Gibbs adsorption theory.

A Generalized Cahn Wetting Model

Cahn (21) analyzed a demixed binary liquid system, using a diffuse-interface model, by finding the spatially varying concentration function [$c(x)$] that minimizes the excess free energy per unit

area of a flat surface:

$$\sigma^x = \Phi(c_s) + \int_0^\infty [\Delta f(c(x)) + \kappa_c \cdot |\nabla c(x)|^2] dx, \qquad\qquad 3.$$

where x is the spatial parameter perpendicular to the surface located at $x = 0$. $\Phi(c_s)$ is the surface term, where c_s is the concentration at the free surface. $\Delta f(c)$ is the homogenous free-energy density referred to equilibrium bulk phases. κ_c is the gradient energy coefficient.

A combination of Cahn's theory for binary liquids with the Kobayashi-Warren-Carter model (78) that includes additional order parameters to represent crystallinity and orientation fields was used to propose a diffuse-interface model for SAFs (16, 17) where the film energy functional is expressed as

$$\sigma^x = \Phi(c_s, \eta_s, \theta_s) + \int_0^\infty \left[\Delta f(\eta(x), c(x)) + \kappa_\eta \cdot |\nabla \eta(x)|^2 + s \cdot g(\eta) \cdot |\nabla \theta(x)| \right.$$
$$\left. + \frac{\beta^2}{2} \cdot |\nabla \theta(x)| + \kappa_c \cdot |\nabla c(x)|^2 \right] dx. \qquad\qquad 4.$$

$\Delta f(\eta, c)$ is the homogenous free-energy density as a function of both concentration [$c(x)$] and crystallinity [$\eta(x)$] fields, but not the orientation field [$\theta(x)$]. Gradient energy coefficients κ_η, κ_c, and s are model parameters to be tuned to experiments and first-principle calculations. $\Phi(c_s, \eta_s, \theta_s)$ is a surface energy term similar to that in Equation 3. Rigorous analysis in a similar model developed by Tang et al. (20) showed that coupled GB prewetting and premelting transitions are possible in a binary alloy. The gradient in orientation ($\nabla \theta$) is probably less important for SAFs than for IGFs that are confined between two crystals. If this term is neglected, Equation 4 can be simplified for a fixed surface orientation, θ_0, as

$$\sigma^x = \Phi(c_s, \eta_s, \theta_0) + \int_0^\infty [\Delta f(\eta(x), c(x)) + \kappa_\eta \cdot |\nabla \eta(x)|^2 + \kappa_c \cdot |\nabla c(x)|^2] dx. \qquad 5.$$

This diffuse-interface model can be used to analyze SAF stability (17), whereupon several surface complexion (phase) diagrams can be deduced (**Figure 10**). [Such nanoscale interfacial features were termed "complexions" by Tang et al. (20) because in a strict sense they are not phases according to Gibbs's definition.] A first-order coupled prewetting and premelting transition (i.e., the dewetting transition at which nanoscale SAFs vanish) can occur in the subeutectic regime. Furthermore, this prewetting line in the solid-solid two-phase regime extends into the single-phase regime, in which the prewetting transition temperature increases with decreasing chemical potential (**Figure 10**). The prewetting line may terminate at either a first-order surface premelting transition point of the pure substrate (**Figure 10a**) or a surface critical point (**Figure 10b**). These predictions are qualitatively consistent with the experimental observations shown in **Figure 4** for Bi_2O_3-enriched SAFs on ZnO. Further refinements of the model for SAFs in ceramic materials should include the effects of dispersion forces, electrostatic interactions, and strain energies.

A recent work (17) used the diffuse-interface theory to explain qualitatively the different sharpnesses at the substrate-adsorbate interfaces. From equation 7 in Cahn's original paper on the critical-point wetting theory for binary demixed liquids (21), the compositional gradient at the transition between the matrix phase and adsorbates is

$$\left| \frac{dc}{dx} \right|_{\text{trans}} = \sqrt{\frac{\Delta E}{\kappa_c}}, \qquad\qquad 6.$$

where ΔE is the height of the potential barrier between the minimum energy states for the two immiscible liquids in the function of free energy versus concentration. Because prewetting occurs at temperatures close to the bulk critical point, ΔE is moderate in value, which results in rather
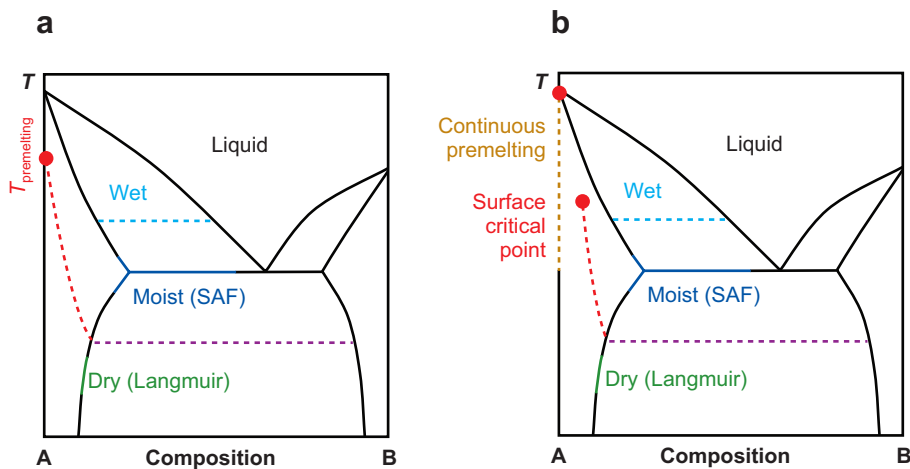
Figure 10

Schematic illustration of a generalized prewetting model. The region of stable nanoscale SAFs is bounded by two transitions. The prewetting line, representing first-order transitions from Langmuir submonolayer adsorption to SAFs, extends from the subeutectic regime into the single-phase region and terminates at (*a*) a first-order surface premelting transition point or (*b*) a surface critical point. Reprinted from Reference 17 with permission from Elsevier.

diffuse interfaces between the adsorbates and the matrix phase. An extension of Equation 6 for binary solid-liquid systems has been deduced (17):

$$\sqrt{\kappa_\eta \cdot \left|\frac{d\eta}{dx}\right|^2_{\text{trans}} + \kappa_c \cdot \left|\frac{dc}{dx}\right|^2_{\text{trans}}} = \sqrt{\Delta E}. \qquad 7.$$

In the case of binary systems with deep eutectic reactions, the free-energy barrier ΔE for the structural transition is high, which should result in abrupt film-crystal transitions. The film-crystal interfaces in HRTEM images of quenched specimens are nearly atomically abrupt (see, e.g., **Figure 6*a***), appearing to support the above argument, although in situ experiments are needed to verify interface configurations.

Force-Balance Models

The apparent existence of abrupt film-substrate interfaces supports the simplified treatment of the film free-energy model as force-balance or pressure-balance models [i.e., a high-temperature colloidal theory (2, 3)], in which through-thickness gradients are largely neglected. The excess free energy of an SAF with thickness h [referred to a mixture of equilibrium bulk phases] is given by (17)

$$G^x(h) = \gamma_{cl} + \gamma_{lv} + \left(\sum_i \Delta\mu_i X_i\right) \cdot \rho \cdot h + \sigma_{\text{interfacial}}(h), \qquad 8.$$

where $\gamma_{cl} + \gamma_{lv}$ represents the sum of crystal-liquid and liquid-vapor interfacial energies. The third thermodynamic term is included for quasi-liquid films formed at subsolidus conditions, where

$$\sum_i \Delta\mu_i X_i \cdot \rho \equiv \Delta G_{\text{vol}} \qquad 9.$$

is the volumetric free energy to form a hypothesized uniform disordered film from a mixture of equilibrium bulk phases. This term is generally the dominant attractive interaction in the subeutectic and undersaturated regions that limits the film thickness. Because volumetric free energy is also considered in the diffuse-interface theories for deriving the short-range forces, this term should be defined consistently in conjunction with the definition of short-range forces (5).

When the film is thin, an extra interfacial free-energy term $\sigma_{\text{interfacial}}(h)$ [i.e., $\omega(l)$ in Dietrich's formulation (28), $P(\zeta)$ in de Gennes's formulation (27), or $E_{\text{int}}(h)$ in Reference 5] arises, representing the total contribution of all interfacial forces. $\sigma_{\text{interfacial}}(h)$ is equal to an integral of the Deryaguin disjoining pressure from h to ∞ (27) and vanishes as $h \to \infty$. For SAFs in oxides, $\sigma_{\text{interfacial}}(h)$ can be expressed as

$$\sigma_{\text{interfacial}}(h) = \frac{-A_{123}}{12\pi h^2} + \sigma_{\text{short-range}}(h) + \sigma_{\text{elec}}(h) + \cdots. \qquad 10.$$

The above equation is similar to the Clarke IGF model (1, 47), except all terms are defined for the configuration of SAFs. The first term is a long-range dispersion interaction, where A_{123} is the Hamaker constant for the sequence of three materials: substrate (1), film (2), and vapor (3). $\sigma_{\text{short-range}}(h)$ is a coupled short-range interaction of structural and chemical origins, and $\sigma_{\text{elec}}(h)$ is an electrostatic interaction. For consistency, all the interfacial free-energy terms are defined so that they vanish as $h \to +\infty$. All σ terms in Equation 10 are free energies.

Then, the excess film free energy as a function of film thickness, referred to the equilibrium bulk phases and the state of $h = 0$, is given by

$$\Delta\sigma(h) \equiv G^x(h) - \gamma_{cv}^{(0)} = \Delta\gamma^{(0)} + (\Delta G_{\text{vol}} \cdot h) + \frac{-A_{123}}{12\pi h^2} + \sigma_{\text{short-range}}(h) + \sigma_{\text{elec}}(h) + \cdots, \qquad 11.$$

with

$$\Delta\gamma^{(0)} \equiv \gamma_{lv} + \gamma_{cl} - \gamma_{cv}^{(0)}. \qquad 12.$$

Here, we use the superscript ($^{(0)}$) to denote that this surface free-energy term is different from the true equilibrium $\Delta\gamma_{eq.}$ (defined in Equation 18). As discussed above, $\gamma_{cv}^{(0)}$ is the excess free energy of a "clean" surface without any adsorption.

Practically, the condition $\Delta\gamma^{(0)} < 0$ is often used as a criterion for complete wetting (5). Rigorously, $\Delta\gamma^{(0)} < 0$ is only a necessary condition for complete wetting; it becomes a sufficient condition if the excess free energy varies monotonically with film thickness. For example, if an equilibrium-thickness SAF represents a global minimum in free energy versus film thickness, $\Delta\gamma^{(0)}$ can be negative, yet complete wetting does not occur. The thermodynamic condition for complete wetting is $\gamma_{cv} \equiv \gamma_{lv} + \gamma_{cl}$ (Equation 2) (5, 27).

It is often assumed that either $\sigma_{\text{short-range}}(h)$ or $\sigma_{\text{elec}}(h)$ is the dominant repulsion; both interactions can be approximated as exponentially decaying forms. Then, a generic repulsion, $K \cdot e^{-h/\xi}$, where ξ is a coherent length for a short-range force or the Debye length κ^{-1} for an electrostatic interaction, can be used for estimating film thickness. Although in principle one can accurately determine the term ΔG_{vol} by considering fusion entropies of both components plus the mixing entropy and enthalpy (e.g., using the database and methods in CALPHAD), the fusion entropy of the film-forming component provides a rough estimate:

$$\Delta G_{\text{vol}} \approx \Delta S_{\text{vol.}}^{\text{fusion}} \cdot \Delta T = \Delta S_{\text{vol.}}^{\text{fusion}} \cdot (T_{\text{eutectic}} - T). \qquad 13.$$

Then, Equation 11 can be rewritten for subeutectic films as

$$\Delta\sigma(h) = \Delta\gamma^{(0)} + \Delta S_{\text{vol}}^{\text{fusion}} \cdot \Delta T \cdot h + \frac{-A_{123}}{12\pi h^2} + K \cdot e^{-h/\xi}. \qquad 14.$$

An equilibrium thickness represents a balance between the attractive and repulsive interfacial pressures/forces, corresponding to a global or local minimum in excess film free energy versus thickness defined by

$$\frac{d[\Delta\sigma(h)]}{dh}\bigg|_{h=h_{eq.}} = 0. \qquad \qquad 15.$$

Equations 8–15 for SAFs can be considered as a free-surface analogy of the Clarke force-balance model for IGFs (1, 47).

Equations 14 and 15 have been used to compute thickness versus temperature for both Bi_2O_3-based SAFs on ZnO and VO_x-based SAFs on TiO_2. For Bi_2O_3-enriched SAFs on ZnO {$11\bar{2}0$} surfaces, the Hamaker constant A_{123} is approximately +137 zJ (attractive dispersion interaction) (15), and $K \approx \Delta\gamma^{(0)}$ is ~-250 mJ m^{-2} (17). It is further assumed that the SAFs in Bi_2O_3-saturated specimens equilibrated slightly above the bulk eutectic temperature are represented by Equation 14 with $\Delta T = 0$, and the equilibrium thickness associated with the minimum free energy in Equation 14 is taken to be equal to the experimentally measured mean value of 1.54 nm, from which ξ is evaluated to be 0.25 nm. **Figure 11** shows the associated curve for excess film free energy versus thickness. Using the fusion entropy value of pure Bi_2O_3 (0.29 mJ·m^{-2}·nm^{-1}·K^{-1})
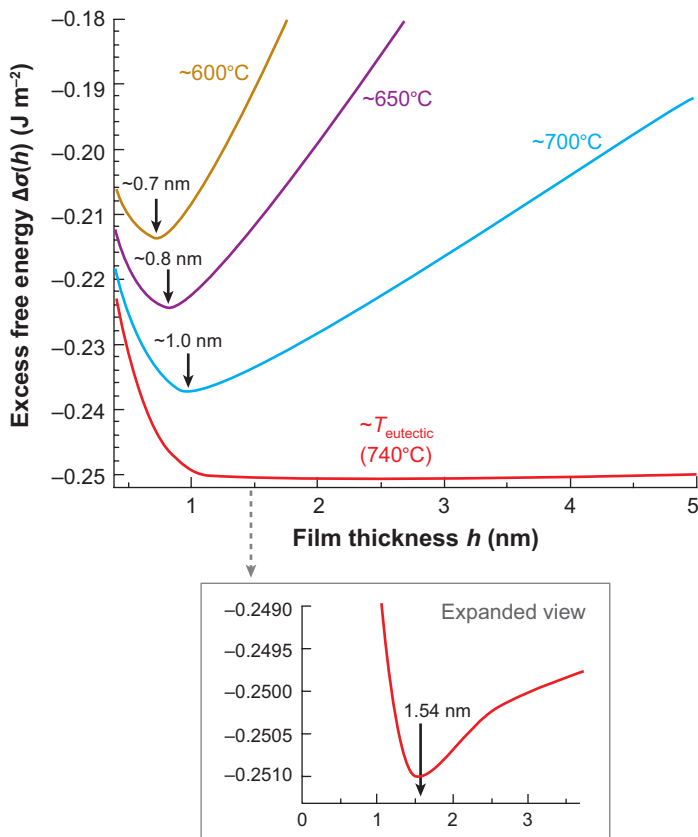
Figure 11

Computed excess film energies versus thickness for Bi_2O_3-enriched SAFs on ZnO. The model in Reference 17 was used to replot this figure.

to estimate the volumetric term, as well as Equation 14, one can compute excess film free energies versus thicknesses. The equilibrium thicknesses at 600°C, 650°C, and 700°C, corresponding to the minima as in **Figure 10**, are 0.7 nm, 0.8 nm, and 1.0 nm, respectively [∼0.1 nm lower than estimates that do not consider the dispersion force (17)]. These results are 0.2–0.3 nm lower than the experimental data, which is in satisfactory agreement given the multiple approximations used. In particular, assuming values for pure Bi_2O_3 in Equation 13 is not absolutely correct because the experiments show that as much as 56 vol.% ZnO dissolves in the SAF at 780°C (with a Bi/Zn cationic ratio of only 0.43) (**Figure 3a**) (15).

A similar calculation was conducted for VO_x-enriched SAFs on TiO_2 (101) surfaces. The solid line in **Figure 6c** was calculated via Equation 14 [but with a modified expression for the dispersion force, $-A_{123}/12\pi(b^2 + \xi_0^2)$, that considers the finite dimension of interatomic distance (ξ_0) to eliminate the singularity at $b = 0$, which is more accurate for thinner films] (18). Again, a reasonable agreement between the computation model and experiments has been demonstrated.

That the above model predicts reasonable equilibrium film thickness versus temperature at the subeutectic regime for both systems suggests that ΔG_{vol} does play a dominant role in determining subeutectic film stability. This hypothesis is also supported by the stabilization of subeutectic SAFs in systems with repulsive dispersion forces, e.g., Bi_2O_3 on Fe_2O_3 and WO_3 on TiO_2 (**Figure 8**) (15). The stabilization of subeutectic quasi-liquid SAFs in binary systems has clear parallels to surface premelting in unary systems.

Wetting in the Presence of Nanoscale Surficial Amorphous Films

If an equilibrium-thickness SAF corresponds to a global minimum in excess free energy,

$$\gamma_{cv} \equiv \gamma_{SAF} = (\gamma_{cl} + \gamma_{lv}) + \sigma_{interfacial}(b_{eq.}).$$ 16.

Combining Equations 16 and 1 gives the Young's contact angle:

$$\cos \theta_Y = \frac{\gamma_{cv} - \gamma_{cl}}{\gamma_{lv}} = 1 - \frac{\Delta\gamma_{eq.}}{\gamma_{lv}},$$ 17.

where

$$\Delta\gamma_{eq.} \equiv -\sigma_{interfacial}(b_{eq.}) \equiv \gamma_{cl} + \gamma_{lv} - \gamma_{SAF} \equiv \gamma_{cl} + \gamma_{lv} - \gamma_{cv}.$$ 18.

$\Delta\gamma_{eq.}(T)$ was estimated for Bi_2O_3-enriched SAFs on ZnO {11$\bar{2}$0} surfaces by combination of Equation 17 and the measured contact angles (**Figure 9c**). **Figure 9d** shows the computed $\Delta\gamma_{eq.}$ versus T. In wetting theories (28), the thickening of an adsorbed SAF (and the associated decrease in the $\Delta\gamma_{eq.}$ and contact angle) with increasing temperature is explained by a competition between entropy and energy. As temperature increases, the liquid-vapor interface would like to avoid the solid-liquid interface, which hinders interfacial fluctuation. A complete wetting transition may occur as the system approaches a critical point, where $b_{eq.} \to \infty$, $\Delta\gamma_{eq.} \to 0$, and $\theta_Y \to 0$. If the wetting transition is first order, $\Delta\gamma_{eq.} \propto (T_W - T)$, $\theta_Y \propto (T_W - T)^{1/2}$, and $b_{eq.}$ jumps discretely to infinity at the wetting temperature T_W. If a critical (continuous) wetting transition occurs, $b_{eq.}$ is divergent continuously at T_W.

For Bi_2O_3 on ZnO, although complete wetting is not observed, a monotonic decrease in contact angle with increasing temperature is evident for drops on the {11$\bar{2}$0} surfaces (**Figure 9c**) in the presence of SAFs. [Moreover, the contact angle is constant for drops on the {1$\bar{1}$00} surfaces (**Figure 9c**) in the absence of SAFs.] This suggests that wetting in the presence of SAFs follows a generalized Cahn wetting theory (i.e., a gradual decrease in $\gamma_{sv} \equiv \gamma_{SAF}$ and thickening of adsorption films with increasing temperature as the system approaches its critical point) (21, 26,

28). Linear extrapolation from the data between 750°C and 800°C would project a first-order complete wetting transition at 818°C (**Figure 9d**).

The inhibition of complete wetting can be explained by the presence of a long-range dispersion force of significant strength. For a Bi_2O_3-rich eutectic liquid film on a ZnO surface, the Hamaker constant for SAFs [$A_{123} = +137$ zJ (15)] is significantly greater than that for IGFs in the same system ($A_{121} \approx 58$ zJ, if a single-oscillator estimation is used). If the dispersion interaction is attractive and is the longest-range force, then complete wetting theoretically cannot occur, as Lipowsky (79) has indicated. An analysis using a continuum model by de Gennes also showed that a long-range force can suppress the complete wetting transition that would otherwise occur as the system approached a critical point (28).

If the equilibrium thickness results from a balance between the dispersion force and a generic, exponentially decaying short-range repulsion, the following relation can be derived:

$$\frac{K}{\xi} \cdot e^{-h_{eq.}/\xi} = \frac{A_{123}}{6\pi h_{eq.}^3}. \qquad 19.$$

Thus,

$$\Delta \gamma_{eq.} \equiv -\sigma_{interfacial}(h_{eq.}) = \frac{A_{123}}{12\pi h_{eq.}^2} - K \cdot e^{-h_{eq.}/\xi} = \frac{A_{123}}{12\pi h_{eq.}^2} \cdot (1 - 2\xi/h_{eq.}). \qquad 20.$$

Equation 17 and Equation 20 were combined to obtain the residual contact angle. The resulting values are $\sim 5.5°$ for a 2-nm-thick SAF and $\sim 3.6°$ for a 3-nm-thick SAF, which are in good agreement with experiment ($4° < \theta_Y < 6°$ at 900–1050°C) and support the interpretation that complete wetting is inhibited by the long-range attractive dispersion force.

SUMMARY POINTS

1. Stable nanometer-thick SAFs are observed for Bi_2O_3 on ZnO, on VO_x on TiO_2, and in several other binary oxides, suggesting that such SAFs occur widely in ceramic systems.

2. The film thickness, corresponding to the Gibbsian excess of solute/adsorbate, increases monotonically with increasing temperature and is reversible upon changes in temperature, consistent with being a thermodynamically determined equilibrium thickness.

3. Stabilization of quasi-liquid SAFs at subeutectic and undersaturated conditions in two-component systems is analogous to the phenomena of surface premelting in unary systems and prewetting in binary demixed liquids.

4. Nanometer-thickness SAFs vanish at a dewetting temperature (i.e., a coupled prewetting and premelting transition temperature) that is well below the bulk eutectic temperature. Observation of a hysteresis in thickness versus temperature suggests that this transition is first order.

5. In the solid-liquid coexistence regime, nanometer-thick SAFs form in equilibrium with partial-wetting drops, analogous to the phenomenon of frustrated-complete wetting.

6. For Bi_2O_3 on ZnO, the macroscopic contact angle of a partial-wetting liquid drop in equilibrium with a nanoscale SAF decreases with increasing temperature but does not go to zero. The absence of complete wetting is attributed to the presence of an attractive dispersion force.

7. Stability and equilibrium thicknesses of SAFs can be explained by a balance between several interfacial forces, including long-range London dispersion forces, short-range interactions of structural and chemical origins, electrostatic interactions, and volumetric free energies.

8. These SAFs can be alternatively considered as disordered multilayer adsorbates in a diffuse-interface theory that is extended from the Cahn critical-point wetting model.

FUTURE ISSUES

1. A quantitative model for predicting SAF stability, structure, and thickness from thermodynamic data for untested systems is needed.

2. It is likely that SAFs play important roles in engineering materials other than those commented on in this review. Opportunities to exploit SAFs with self-selecting thickness, composition, and structure in applications such as ultrathin dielectric films, supported oxide catalysts, device junctions, and morphology control of nanocrystals, among other areas, should be explored.

3. The detailed atomic structure of SAFs, including the nature of partial order, is not well understood. Do layering transitions exist? In situ hot-stage experiments could help us understand the behavior of SAFs at temperatures of equilibration.

4. In principle, two distinct surface transitions, from monolayer adsorption to nanoscale SAFs, and from nanoscale SAFs to complete wetting transitions, can exist. Furthermore, other more complex surface transitions may also exist. These surface transitions can result in abrupt changes in properties, and further work is needed to confirm and elaborate these transitions. For example, if the dispersion force is repulsive, does a complete wetting transition universally exist at higher temperature? Are these transitions first order or continuous? Although observation of a hysteresis loop in thickness versus temperature suggests that the transition from Langmuir submonolayer adsorption to nanoscale SAFs may be first order, a direct confirmation is needed.

DISCLOSURE STATEMENT

The authors are not aware of any biases that might be perceived as affecting the objectivity of this review.

ACKNOWLEDGMENTS

LITERATURE CITED

1. **Clarke DR. 1987. On the equilibrium thickness of intergranular glass phases in ceramic materials. *J. Am. Ceram. Soc.* 70:15–22**

2. Cannon RM, Esposito L. 1999. High temperature colloidal behavior: particles in liquid silicates. *Z. Metall.* 90:1002–15

3. **Cannon RM, Rühle M, Hoffmann MJ, French RH, Gu H, et al. 2000. Adsorption and wetting mechanisms at ceramic grain boundaries. In *Grain Boundary Engineering in Ceramics*, ed. T Sakuma, Y Ikuhara, pp. 427–44. Westerville, OH: Am. Ceram. Soc.**

4. Subramaniam A, Koch CT, Cannon RM, Rühle M. 2006. Intergranular glassy films: an overview. *Mater. Sci. Eng. A* 422:3–18

5. **Luo J. 2007. Stabilization of nanoscale quasi-liquid interfacial films in inorganic materials: a review and critical assessment. *Crit. Rev. Solid State Mater. Sci.* 32:67–109**

6. Avishai A, Scheu C, Kaplan WD. 2005. Intergranular films at metal-ceramic interfaces. Part I. Interface structure and chemistry. *Acta Mater.* 53:1559–69

7. Scheu C, Dehm G, Kaplan WD. 2000. Equilibrium amorphous silicon-calcium-oxygen films at interfaces in copper-alumina composite prepared by melt infiltration. *J. Am. Ceram. Soc.* 84:623–30

8. Avishai A, Kaplan WD. 2004. Intergranular films in metal-ceramic composites and the promotion of metal particle occlusion. *Z. Metall.* 95:266–70

9. Avishai A, Scheu C, Kaplan WD. 2003. Amorphous films at metal/ceramic interfaces. *Z. Metall.* 94:272–76

10. Baram M, Kaplan WD. 2006. Intergranular films at Au-sapphire interfaces. *J. Mater. Sci.* 41:7775–84

11. Jeong HG, Hiraga K, Mabuchi M, Higashi K. 1996. Interface structure of Si_3N_4-whisker-reinforced Al-Mg-Si alloy (Al alloy 6061) composites studied by high resolution electron microscopy. *Philos. Mag. Lett.* 74:73–80

12. Luo J, Gupta VK, Yoon DH, Meyer HM. 2005. Segregation-induced grain boundary premelting in nickel-doped tungsten. *Appl. Phys. Lett.* 87:231902

13. Gupta VK, Yoon DH, Meyer HM III, Luo J. 2007. Thin intergranular films and solid-state activated sintering in nickel-doped tungsten. *Acta Mater.* 55:3131–42

14. Luo J, Chiang Y-M. 1999. Equilibrium-thickness amorphous films on {11-20} surfaces of Bi_2O_3-doped ZnO. *J. Eur. Ceram. Soc.* 19:697–701

15. **Luo J, Chiang Y-M. 2000. Existence and stability of nanometer-thick disordered films on oxide surfaces. *Acta Mater.* 48:4501–15**

16. **Luo J, Chiang Y-M, Cannon RM. 2005. Nanometer-thick surficial films in oxides as a case of prewetting. *Langmuir* 21:7358–65**

17. **Luo J, Tang M, Cannon RM, Carter WC, Chiang Y-M. 2006. Pressure-balance and diffuse-interface models for surficial amorphous films. *Mater. Sci. Eng. A* 422:19–28**

18. **Qian H, Luo J. 2007. Vanadia-based equilibrium-thickness amorphous films on anatase (101) surfaces. *Appl. Phys. Lett.* 91:061909**

19. Tang M, Ramos A, Jud E, Chung S-Y, Gautier-Soyer M, et al. 2008. Nanometer-scale wetting of the silicon surface by its equilibrium oxide. *Langmuir*. In press

20. Tang M, Carter WC, Cannon RM. 2006. Grain boundary transitions in binary alloys. *Phys. Rev. Lett.* 97:075502

21. **Cahn JW. 1977. Critical point wetting. *J. Chem. Phys.* 66:3667–72**

22. Dash JG. 1989. Surface melting. *Contemp. Phys.* 30:89–100

23. Dash JG, Fu H, Wettlaufer JS. 1995. The premelting of ice and its environmental consequences. *Rep. Prog. Phys.* 58:115–67

24. Dash JG, Rempel AM, Wettlaufer JS. 2006. The physics of premelted ice and its geophysical consequences. *Rev. Mod. Phys.* 78:695–741

1. The original theory on equilibrium thickness of IGFs in ceramics.

3. Assessed IGFs in several ceramic systems.

5. Assessed ceramic IGFs, their metallic and free-surface counterparts, prewetting, premelting, and frustrated-complete wetting in a unifying thermodynamic framework.

15. Reported the equilibrium thickness, distinct composition, and anisotropic formation of Bi_2O_3-enriched SAFs on ZnO and SAFs in systems with repulsive dispersion forces.

16. Revealed the reversible thickness-temperature dependence for Bi_2O_3-enriched SAFs on ZnO.

17. Introduced force-balance and diffuse-interface models for SAFs.

18. Studied VO_x-based SAFs on TiO_2 and observed a hysteresis loop in thickness-versus-temperature curve as an indication to a first-order transition.

21. The critical-point wetting model that suggested the existence of wetting and prewetting transitions.

25. Observed anisotropic wetting with and without SAFs and revealed the inhibition of complete wetting by an attractive London dispersion force.

27. An in-depth discussion of wetting phenomena.

25. **Qian H, Luo J, Chiang Y-M. 2008. Anisotropic wetting of ZnO by Bi$_2$O$_3$ with and without nanometer-thick surficial amorphous films.** *Acta Materialia*. **56:862–73**

26. Bonn D, Ross D. 2001. Wetting transitions. *Rep. Prog. Phys.* 64:1085–163

27. **de Gennes PG. 1985. Wetting: statics and dynamics.** *Rev. Mod. Phys.* **57:827–63**

28. Dietrich S. 1988. Wetting phenomena. In *Phase Transitions and Critical Phenomena*, ed. C Domb, JL Lebowitz, pp. 1–218. London: Academic

29. Kellay H, Bonn D, Meunier J. 1993. Prewetting in a binary liquid mixture. *Phys. Rev. Lett.* 71:2607–10

30. Schmidt JW, Moldover MR. 1986. A search for the prewetting line. *J. Chem. Phys.* 84:4563–68

31. Chatain D, Wynblatt P. 1996. Experimental evidence for a wetting transition in liquid Ga-Pb alloys. *Surf. Sci.* 345:85–90

32. Wynblatt P, Chatain D. 1998. Wetting and prewetting transitions in Ga-Pb alloys. *Ber. Bunsenges. Phys. Chem. Chem. Phys.* 102:1142–50

33. Pandit R, Schick M, Wortis M. 1982. Systematics of multilayer adsorption phenomena on attractive substrates. *Phys. Rev. B* 26:5112–20

34. Denesyuk NA, Hansen JP. 2004. Wetting transitions of ionic solutions. *J. Chem. Phys.* 121:3613–24

35. van der Veen JF, Pluis B, Denier AW. 1988. Surface melting. In *Chemistry and Physics of Solid Surfaces*, ed. R Vanselow, RF Howe, pp. 455–67. Berlin: Springer

36. Engemann S, Reichert H, Dosch H, Bilgram J, Honkimaki V, Snigirev A. 2004. Interfacial melting of ice in contact with SiO$_2$. *Phys. Rev. Lett.* 92:205701

37. Dahmen U, Hagege S, Faudot F, Radetic T, Johnson E. 2004. Observations of interface premelting at grain-boundary precipitates of Pb in Al. *Philos. Mag.* 84:2651–62

38. Keblinski P, Wolf D, Phillpot SR, Gleiter H. 1999. Self diffusion in high-angle FCC metal grain boundaries by molecular dynamics simulation. *Philos. Mag. A* 79:2735–61

39. Phillpot SR, Wang J, Wolf D, Gleiter H. 1995. Computer simulation of the structure and dynamical properties of grain boundaries in a nanocrystalline model material. *J. Eng. Appl. Sci. A* 204:76–82

40. von Alfthan S, Haynes PD, Kaski K, Sutton AP. 2006. Are the structures of twist grain boundaries in silicon ordered at 0 K? *Phys. Rev. Lett.* 96:055505

41. von Alfthan S, Kaski K, Sutton AP. 2006. Order and structural units in simulations of twist grain boundaries in silicon at absolute zero. *Phys. Rev. B* 74:134101

42. Benatov L, Wettlaufer JS. 2004. Abrupt grain boundary melting in ice. *Phys. Rev. E* 70:061606

43. Lobkovsky AE, Warren JA. 2002. Phase field model of premelting of grain boundaries. *Physica D* 164:202–12

44. Tang M, Carter WC, Cannon RM. 2006. Diffuse interface model for structural transitions of grain boundaries. *Phys. Rev. B* 73:024102

45. Hsieh TE, Balluffi RW. 1989. Experimental study of grain boundary melting in aluminum. *Acta Metall.* 37:1637–44

46. Alsayed AM, Islam MF, Zhang J, Collings PJ, Yodh AG. 2005. Premelting at defects within bulk colloidal crystals. *Science* 309:1207–10

47. Clarke DR, Shaw TM, Philipse AP, Horn RG. 1993. Possible electrical double-layer contribution to the equilibrium thickness of intergranular glass films in polycrystalline ceramics. *J. Am. Ceram. Soc.* 76:1201–4

48. French RH. 2000. Origin and applications of London dispersion forces and Hamaker constants in ceramics. *J. Am. Ceram. Soc.* 83:2117–46

49. Ackler HD, Chiang Y-M. 1999. Effect of initial microstructure on final intergranular phase distribution in liquid phase sintered ceramics. *J. Am. Ceram. Soc.* 82:183–89

50. Bobeth M, Clarke DR, Pompe W. 1999. Diffuse interface description of intergranular films in polycrystalline ceramics. *J. Am. Ceram. Soc.* 82:1537–46

51. Wang H, Chiang Y-M. 1998. Thermodynamic stability of intergranular amorphous films in bismuth-doped zinc oxide. *J. Am. Ceram. Soc.* 81:89–96

52. Avishai A, Kaplan WD. 2005. Intergranular films at metal-ceramic interfaces. Part II. Calculation of Hamaker coefficient. *Acta Mater.* 53:1571–81

53. Chang LS, Rabkin E, Straumal BB, Baretzky B, Gust W. 1999. Thermodynamic aspects of the grain boundary segregation in Cu(Bi) alloys. *Acta Mater.* 47:4041–46

54. Chang L-S, Rabkin EI, Straumal B, Lejcek P, Hofmann S, Gust W. 1997. Temperature dependence of the grain boundary segregation of Bi in Cu polycrystals. *Scripta Metall. Mater.* 37:729–35

55. Straumal BB, Baretzky B. 2004. Grain boundary phase transitions and their influence on properties of polycrystals. *Interface Sci.* 12:147–55

56. Straumal BB, Zieba P, Gust W. 2001. Grain boundary phase transitions and phase diagrams. *Int. J. Inorg. Mater.* 3:1113–15

57. Divinski S, Lohmann M, Herzig C. 2004. Grain boundary diffusion and segregation of Bi in Cu: radiotracer measurements in B and C regimes. *Acta Mater.* 52:3973–82

58. Divinski S, Lohmann M, Herzig C, Straumal B, Baretzky B, Gust W. 2005. Grain boundary melting phase transition in the Cu-Bi system. *Phys. Rev. B* 71:104104

59. Straumal BB, Noskovich OI, Semenov VN, Shvindlerman LS, Gust W, Predel B. 1992. Premelting transition on 38° <100> tilt grain boundaries in (Fe-10 at.% Si)-Zn alloys. *Acta Metall. Mater.* 40:795–801

60. Rabkin EI, Semenov VN, Shvindlerman LS, Straumal BB. 1991. Penetration of tin and zinc along tilt grain boundaries 43° [100] in Fe-5 at.% Si alloy: premelting phase transition? *Acta Metall. Mater.* 39:627–39

61. Noskovich OI, Rabkin EI, Semenov VN, Straumal BB, Shvindlerman LS. 1991. Wetting and premelting phase transitions in 38° [100] tilt grain boundary in (Fe-12 at.% Si)-Zn alloy in the vicinity of the A_2-B_2 bulk ordering in Fe-12 at.% Si alloy. *Acta Metall. Mater.* 39:3091–98

62. Straumal BB, Rabkin E, Lojkowski W, Gust W, Shvindlerman LS. 1997. Pressure influence on the grain boundary wetting phase transition in Fe-Si alloys. *Acta Mater.* 45:1931–40

63. Wachs IE, Briand LE, Jehng JM, Burcham L, Gao XT. 2000. Molecular structure and reactivity of the group V metal oxides. *Catal. Today* 57:323–30

64. Wachs IE, Weckhuysen BM. 1997. Structure and reactivity of surface vanadium oxide species on oxide supports. *Appl. Catal. A* 157:67–90

65. Xie Y-C, Tang Y-Q. 1990. Spontaneous monolayer dispersion of oxides and salts onto surfaces of supports: applications to heterogeneous catalysis. *Adv. Catal.* 31:1–43

66. Weckhuysen BM, Keller DE. 2003. Chemistry, spectroscopy and the role of supported vanadium oxides in heterogeneous catalysis. *Catal. Today* 78:25–46

67. Centi G. 1996. Nature of active layer in vanadium oxide supported on titanium oxide and control of its reactivity in the selective oxidation and ammoxidation of alkylaromatics. *Appl. Catal. A* 147:267–98

68. Sanati M, Wallenberg RL, Andersson A, Jansen S, Tu Y. 1991. Vanadia catalysts on anatase, rutile, and TiO_2(B) for the ammoxidation of toluene: an ESR and high-resolution electron microscopy characterization. *J. Catal.* 132:128–44

69. Habel D, Stelzer JB, Feike E, Schroder C, Hosch A, et al. 2006. Phase development in the catalytic system V_2O_5/TiO_2 under oxidising conditions. *J. Eur. Ceram. Soc.* 26:3287–94

70. Gates B, Wu Y, Yin Y, Yang P, Xia Y. 2001. Single-crystalline nanowires of Ag_2Se can be synthesized by templating against nanowires of trigonal Se. *J. Am. Chem. Soc.* 123:11500–1

71. Kong XY, Ding Y, Wang ZL. 2004. Metal-semiconductor Zn-ZnO core-shell nanobelts and nanotubes. *J. Phys. Chem. B* 108:570–74

72. Kuykendall T, Pauzauskie P, Lee S, Zhang Y, Goldberger J, Yang P. 2003. Metalorganic chemical vapor deposition route to GaN nanowires with triangular cross sections. *Nano Lett.* 3:1063–66

73. Xu TT, Zheng J-G, Nicholls AW, Stankovich S, Piner RD, Ruoff RS. 2004. Single-crystal calcium hexaboride nanowires: synthesis and characterization. *Nano Lett.* 4:2051–55

74. Feng X, Sayle DS, Wang ZL, Paras MS, Santora B, et al. 2006. Converting ceria polyhedral nanoparticles into single-crystal nanospheres. *Science* 312:1504–8

75. Cheng W-C, Chatain D, Wynblatt P. 1995. Observations of anisotropic wetting in solid-liquid Pb-Ga alloys. *Surf. Sci.* 327:501–4

76. Chatain D, Metois JJ. 1993. New procedure for the determination of free energies of solid-fluid interfaces from the anisotropy of wetting of a melt on its solid. *Surf. Sci.* 291:1–13

77. Bertrand E, Dobbs H, Broseta D, Indekeu J, Bonn D, Meunier J. 2000. First-order and critical wetting of alkanes on water. *Phys. Rev. Lett.* 85:1282–85

78. Kobayashi R, Warren JA, Carter WC. 2000. A continuum model of grain boundaries. *Physica D* 140:141–51

79. Lipowsky R. 1986. Melting at grain boundaries and surfaces. *Phys. Rev. Lett.* 57:2876